

# Prediction on the Mechanical and Forming Behavior of DP590 Steel Based on a Flow Model

Rui-bin GOU<sup>1,2,3</sup>, Wen-jiao DAN<sup>1,3\*</sup>, Wei-gang ZHANG<sup>1,3</sup>, Min YU<sup>4</sup>

<sup>1</sup> Department of Engineering Mechanics, Shanghai Jiao Tong University, Shanghai 200240, China

<sup>2</sup> School of Mechanical Engineering, Anhui Science and Technology University, Bengbu 233100, Anhui, China

<sup>3</sup> Innovation Center for Advanced Ship and Deep-Sea Exploration, Shanghai Jiao Tong University, Shanghai 200240, China

<sup>4</sup> College of Architecture, Anhui Science and Technology University, Bengbu 233100, Anhui, China

crossref <http://dx.doi.org/10.5755/j01.ms.26.4.22104>

Received 20 November 2018; accepted 10 July 2019

An innovative flow model incorporating the mixture hardening law, anisotropic yield function, and incremental strain formulations was elaborated and applied to DP590 ferrite-martensite dual phase steel. To verify the flow model, both the macro/micro stress-strain responses and the forming patterns of DP590 steel with different martensite contents were simulated during the processes of the cup deep-drawing and the unconstrained cylindrical bending to evaluate the influence of martensite content on the mechanical and forming behavior of the steel. It was found that martensite content has a significant impact on the macro/micromechanical and forming behavior of the steel, i.e., the ferrite and steel effective stresses and the effective macro/micro-strain distribution in the cup. Under the unconstrained cylindrical bending, the simulated effective maximum macro/micro-strains were in good agreement with the calculated results from the mixture law-based model. It was concluded that the Buaschinger effect is the main reason for an 8 % error between the simulated and experimental results. The flow model was proved to predict the macro/micro flow and forming behavior of the dual phase steels with a good accuracy.

**Keywords:** stress-strain response, deep-drawing cup forming, unconstrained cylindrical bending, ferrite-martensite dual phase steel.

## 1. INTRODUCTION

Multiple-phase advanced high strength steels including ferrite-martensite dual phase (DP) steels and transformation-induced plasticity (TRIP) steels have been used mainly in the manufacture of the auto-parts and structures due to their excellent mechanical and forming behavior. Because of the heterogeneous characteristics in their microstructure, the mechanical responses of these multiple-phase high strength steels (especially for micromechanical properties) cannot be predicted reasonably and precisely.

However, some methods and models were developed to solve this problem in describing the material mechanical properties, e.g., the representative volume element (RVE) method [1–8] and the inclusion theory [9–15]. Moreover, many studies about the macro/micromechanical properties of TRIP and DP steels were conducted according to the Mori-Tanaka [10] and the self-consistent schemes, e.g., Tsuchida and Tomota [16], Garion et al. [17], Skoczen [18], Delannay et al. [19], Sitko et al. [20], X. Peng et al. [21], Berbenni et al. [22], Jia et al. [23], Franz et al. [24], Long et al. [25], and Fan [26].

In this paper, a flow model for the multi-phase high strength steels was investigated in details to evaluate the macro/micro stress-strain responses and the forming behavior of these multi-phase high strength steels based on the continuum mechanics theory. The flow model includes

a mixture strain hardening law, a mixture anisotropic yield function, and an incremental formulation, respectively. To describe the macro/micro stress-strain responses of the ferrite-martensite DP steel, the flow model was employed in the ABAQUS/UMAT code. The forming behavior of DP590 steel was simulated during the processes of the cup deep-drawing and the unconstrained cylindrical bending tests. The accuracy of the model was verified by comparing the simulated spring-back angle with the experimental value and the value given in Lee's work [27].

## 2. THEORY MODEL

### 2.1. Mixture hardening law

Based on the strain partitioning between the soft and the hard constituents [19], the strain hardening model [20], the stress flow of DP600 steel in dynamic tensile [28] and the strain distributions within the ferrite-martensite microstructure [29–31], Dan et al. [32] developed a multi-phase stress-strain relationship to study the mechanical behavior of DP and TRIP steels, the mixture strain hardening law is simplified as:

$$\bar{\sigma} = \sum f_i R_i \bar{\sigma}_i, \quad (1)$$

where  $f_i$ ,  $\bar{\sigma}_i$  and  $R_i$  are the individual phase volume fraction, the individual phase stress and the material parameter, respectively.

The stress-strain relationship of individual phase obeys the classical Swift law. Therefore, the stress of individual phase can be written as

\* Corresponding author. Tel.: +86-21-34203084.  
E-mail address: [wjdan@sjtu.edu.cn](mailto:wjdan@sjtu.edu.cn) (W. Dan)

$$\bar{\sigma}_i = k_i (\mathbf{a}_i + \bar{\varepsilon}_i)^{n_i}, \quad (2)$$

where  $k_i$ ,  $a_i$  and  $n_i$  are the materials parameters.

The individual phase effective strain  $\bar{\varepsilon}_i$  is supposed to be controlled by the overall effective strain of material  $\bar{\varepsilon}$  [32]:

$$\bar{\varepsilon}_i = \mathbf{b}_i \bar{\varepsilon}, \quad (3)$$

where  $b_i$  is the strain coefficient of individual phase which is described as

$$\mathbf{b}_i = \exp(\mathbf{p}_{i1} + \mathbf{p}_{i2} \varepsilon), \quad (4)$$

where  $\mathbf{p}_{i1}$  and  $\mathbf{p}_{i2}$  are the parameters of the material.

The hardening rate of the material is described as

$$\mathbf{H}' = \sum f_i \mathbf{R}_i \frac{d\bar{\sigma}_i}{d\bar{\varepsilon}_i} \frac{d\bar{\varepsilon}_i}{d\bar{\varepsilon}} = \sum f_i \mathbf{R}_i \mathbf{b}_i' \frac{d\bar{\sigma}_i}{d\bar{\varepsilon}_i}, \quad (5)$$

where  $\mathbf{b}_i' = \frac{d\bar{\varepsilon}_i}{d\bar{\varepsilon}}$  is the material parameter.

The hardening rate of individual phase can be described as

$$\mathbf{H}'_i = \frac{d\bar{\sigma}_i}{d\bar{\varepsilon}_i}. \quad (6)$$

## 2.2. Anisotropic yield function

For the ferrite-martensite DP steel sheet, the yield function can be defined using the anisotropic coefficient matrix  $M$ , as shown in Eq. 7.

$$\varphi = \sqrt{\sigma^T M \sigma} - \bar{\sigma} = 0. \quad (7)$$

Therefore, the individual phase yield function can be written in a similar form as

$$\varphi_i = \sqrt{\sigma_i^T M \sigma_i} - \bar{\sigma}_i = 0. \quad (8)$$

According to Eq. 1, Eq. 7 and Eq. 8, the material yield function can be rewritten as

$$\varphi = \sum f_i \mathbf{R}_i \varphi_i = \sum B_i \varphi_i. \quad (9)$$

## 2.3. Constitutive model

The elasto-plastic deformation of the ferrite-martensite DP steel can be described as

$$\dot{\varphi} = \sum \left( \frac{\partial \varphi}{\partial B_i} \dot{B}_i + \frac{\partial \varphi}{\partial \varphi_i} \dot{\varphi}_i \right), \quad (10)$$

where  $\frac{\partial \varphi}{\partial B_i} = \varphi_i = 0$ ,  $\frac{\partial \varphi}{\partial \varphi_i} = B_i$  and  $\dot{\varphi}_i = \frac{\partial \varphi_i}{\partial \sigma_i} \dot{\sigma}_i - \mathbf{H}'_i \dot{\varepsilon}_i^p$ .

Thus, Eq. 10 can be simplified as

$$\dot{\varphi} = \sum B_i \left( \frac{\partial \varphi_i}{\partial \sigma_i} \dot{\sigma}_i - \mathbf{H}'_i \dot{\varepsilon}_i^p \right), \quad (11)$$

where  $H_i$  and  $\dot{\sigma}_i$  are the hardening rate and the stress increment of individual phase, respectively.

The stress increment of individual phase  $\dot{\sigma}_i$  can be described using the modulus matrix  $D_i^e$ , the individual

phase strain  $\dot{\varepsilon}_i$  and the plastic strain increment  $\dot{\varepsilon}_i^p$  of individual phase as

$$\dot{\sigma}_i = D_i^e (\dot{\varepsilon}_i - \dot{\varepsilon}_i^p). \quad (12)$$

Based on the associated plastic flow rule, the individual phase strain increment  $\dot{\varepsilon}_i$  and its plastic strain increment  $\dot{\varepsilon}_i^p$  can be expressed by the material strain increments  $\dot{\varepsilon}$  and  $\dot{\varepsilon}^p$  respectively.

$$\dot{\varepsilon}_i = \frac{\partial \varphi_i}{\partial \sigma_i} \dot{\varepsilon}_i^p = \frac{\partial \varphi_i}{\partial \sigma_i} \mathbf{b}'_m \dot{\varepsilon}^p = \frac{\partial \varphi_i}{\partial \sigma_i} \mathbf{b}'_m \frac{\sigma}{\bar{\sigma}} \dot{\varepsilon}; \quad (13)$$

$$\dot{\varepsilon}_i^p = \frac{\partial \varphi_i}{\partial \sigma_i} \dot{\varepsilon}_i^p = \frac{\partial \varphi_i}{\partial \sigma_i} \mathbf{b}'_m \dot{\varepsilon}^p = \frac{\partial \varphi_i}{\partial \sigma_i} \mathbf{b}'_m \frac{\sigma}{\bar{\sigma}} \dot{\varepsilon}^p. \quad (14)$$

For the associated plastic flow rule, the effective plastic strain increment of the material  $\dot{\varepsilon}^p$  can be described as:

$$\dot{\varepsilon}^p = \dot{\lambda} \frac{\partial \varphi}{\partial \sigma} \quad (\dot{\varepsilon}^p = \dot{\lambda}). \quad (15)$$

Substituting Eq. 12, Eq. 13, Eq. 14 and Eq. 15 into Eq. 11, we can get that:

$$\dot{\varphi} = \sum B_i \mathbf{b}'_i \left( \frac{\partial \varphi_i}{\partial \sigma_i} D_i^e \frac{\partial \varphi_i}{\partial \sigma_i} \frac{\sigma}{\bar{\sigma}} \left( \dot{\varepsilon} - \dot{\lambda} \frac{\partial \varphi}{\partial \sigma} \right) - \mathbf{H}'_i \dot{\lambda} \right) = 0. \quad (16)$$

Finally, the increment of the plastic strain in the multi-phase steel can be described as:

$$\dot{\varepsilon}^p = \left( \frac{\sum B_i \mathbf{b}'_i \frac{\partial \varphi_i}{\partial \sigma_i} D_i^e \frac{\partial \varphi_i}{\partial \sigma_i}}{\sum B_i \mathbf{b}'_i \left( \frac{\partial \varphi_i}{\partial \sigma_i} D_i^e \frac{\partial \varphi_i}{\partial \sigma_i} + \mathbf{H}'_i \right)} \right) \dot{\varepsilon}. \quad (17)$$

## 3. MATERIAL

The 1.0 mm thick 0.112 wt.% C, 1.428 wt.% Mn, 0.39 wt.% Si, 0.011 wt.% P, 0.011 wt.% S DP590 steel sheet was employed in present work. Elastic modulus, yield strength and tensile strength of the material were 205 GPa, 409 MPa and 600 MPa, respectively. The uniform and total elongations of the steel were 17.11 % and 31.01 % respectively. The volume fractions of ferrite and martensite phases ( $f_i$ ) in DP590 steel was approximately evaluated using the investigated microstructure (as shown in Fig. 1), and they are 84.2 % for ferrite and 15.8 % for martensite, respectively. According to works of Dan et al. [32–34], the corresponding material parameters referring to  $k_i$ ,  $a_i$ ,  $n_i$ ,  $p_{i1}$  and  $p_{i2}$  are given in Table 1.

**Table 1.** Material parameters of DP590 steel for the proposed model [34]

Individual phase	$k_i$ , MPa	$a_i$	$n_i$	$p_{i1}$	$p_{i2}$	$R_i$
Ferrite	746	0.002	0.19	0.1426	-0.2349	1.12
Martensite	2478	$10^{-7}$	0.52	-1.0853	0.3172	1.45

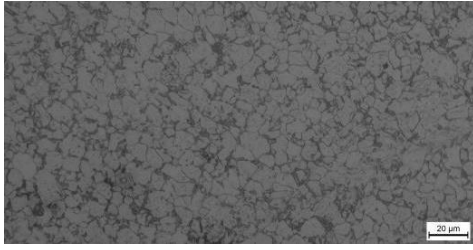


Fig. 1. The investigated microstructure of DP590 steel

## 4. RESULTS AND DISCUSSION

Using the ABAQUS/UMAT code, solid element with the reduced integration (C3D8R) was employed in the following simulations. Under tensile test, the model validity was verified by Dan et al. [34] and Tasan et al. [30]. It was found that the model can predict the macro/micromechanical properties of DP590 steel precisely, i.e., the strain energy densities of ferrite and martensite phases, the stress-strain responses of the material, ferrite phase, and martensite phase.

### 4.1. Cup deep-drawing forming

The cup deep-drawing simulation has been carried out, and the geometry of the cup forming is shown in Fig. 2. The diameter of the steel sheet blank is 200 mm, the thickness of the blank is 1.0 mm, and the punch stroke is 40 mm. The anisotropic coefficients for the mixture yield function in Eq. 8 are  $F_i = 0.436$ ,  $G_i = 0.44$ ,  $H_i = 0.56$ ,  $M_i = 1.0$ ,  $N_i = 1.524$  and  $L_i = 1.0$ , respectively. The blank-holder force is 50 kN. The friction coefficient is assumed to be 0.15 for the blank-punch contact and 0.10 for both the blank-die and the blank-holder contacts.

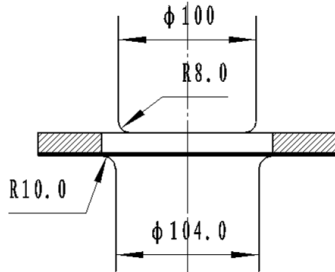


Fig. 2. The dimension of cup drawing tools

The effective stress/strain distribution of the material

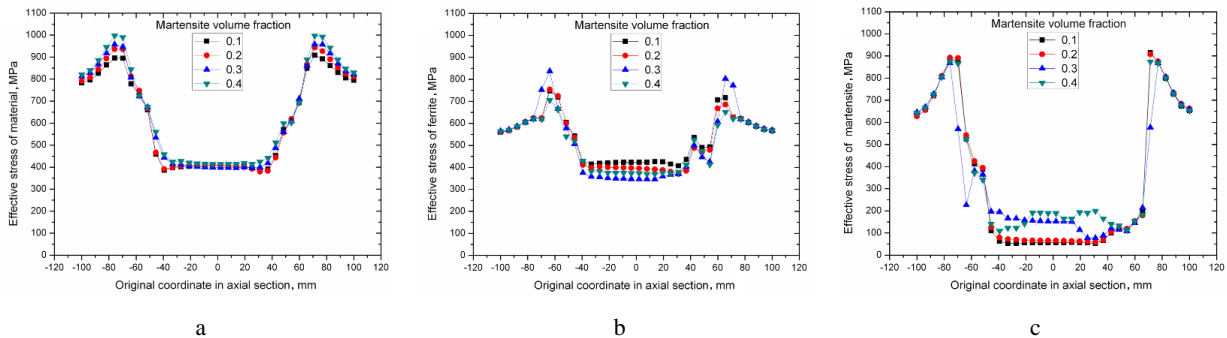


Fig. 4. The effective stress distribution of the material and individual phase with different martensite volume fractions: a – material; b – ferrite; c – martensite

and two individual phases after the cup deep-drawing forming is shown in Fig. 3.

In Fig. 3, after the deep-drawing forming, the maximum effective stress occurs in the martensite phase at the upper corner of the cup (i.e., die round), while the maximum effective strain happens in ferrite phase at the same location of the cup. The stress and strain distribution of the material is similar to that of the ferrite phase. This result shows that martensite and ferrite are largely responsible for the stress and strain distribution of the material.

To investigate the influence of the martensite volume fraction on the stress-strain responses of the material and individual phase, the effective stress/strain distribution of the material and individual phase were calculated when the martensite volume fraction is equal to 0.1, 0.2, 0.3 and 0.4, respectively. The simulated results are shown in Fig. 4 and Fig. 5, respectively.

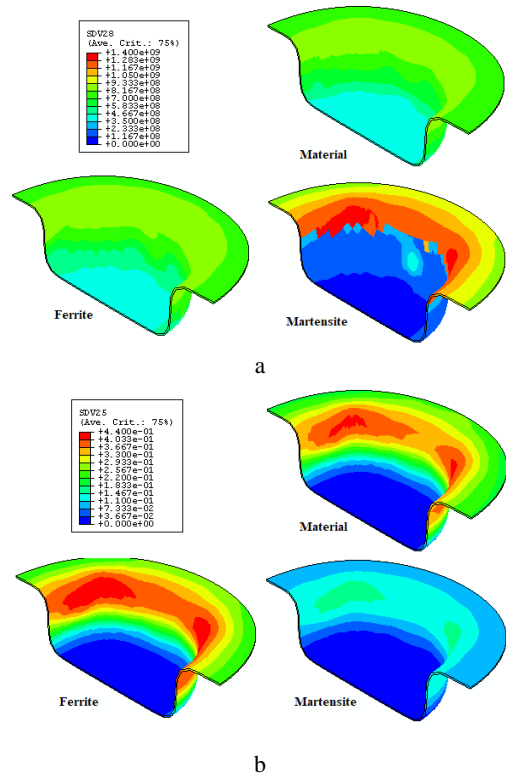
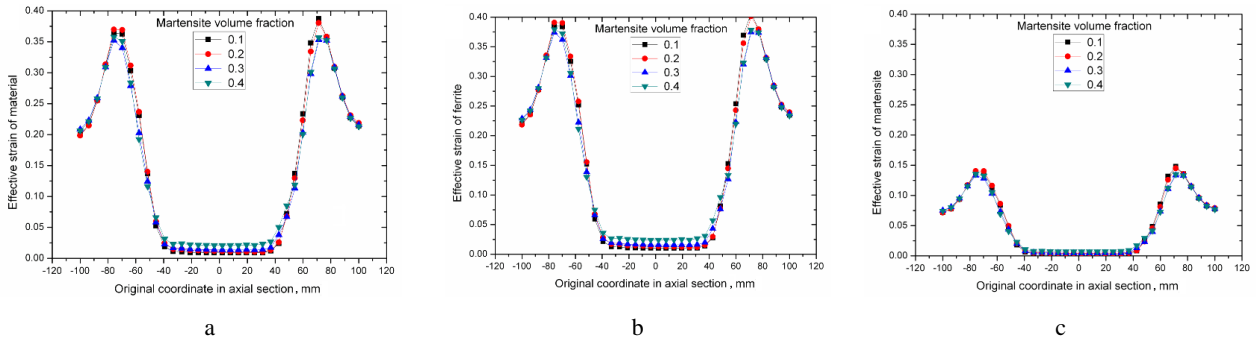


Fig. 3. The effective stress/strain distribution of the material and two individual phases after the cup deep-drawing forming: a – stress; b – strain



**Fig. 5.** The effective strain distribution of the material and individual phase with different martensite volume fractions: a – material; b – ferrite; c – martensite

As seen in Fig. 4 and Fig. 5, with an increase of the martensite volume fraction: (1) the effective stresses of the material and martensite increase, while the ferrite effective stress decreases except for  $f_m = 0.3$  (Fig. 4); (2) the effective strains of the material and individual phase increase both at the bottom and the bottom corner (i.e., punch round) of the cup, but decrease at the upper corner (i.e., die round) and the side wall of the cup (Fig. 5).

The decrease in the effective strain in the cup upper corner reveals that the increment of martensite content worsens the formability of the steel. The increase in effective stress at the bottom of the cup further proves that martensite can improve the strength of the material.

#### 4.2. Unconstrained cylindrical bending

The unconstrained cylindrical bending system which is without blank holders is shown in Fig. 6. The initial dimension of the steel blank was 120.0 mm in length and 30.0 mm in width. The initial position of the punch barely makes a contact with the blank sheet, and the total stroke of the punch is 27.5 mm.

The measuring method of the spring-back angle for the bending test agrees with the requirements of references [27, 35]. The friction coefficient was assumed to be a constant of 0.1 in the simulation.

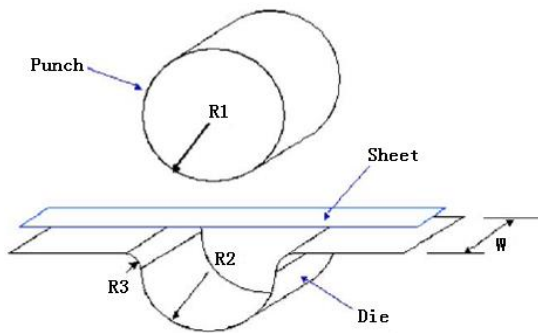


**Fig. 6.** The unconstrained cylindrical bending system ( $R1 = 23.5$  mm;  $R2 = 25.5$  mm;  $R3 = 4.0$  mm)

The simulated strain distribution of the material and individual phase after spring-back is shown in Fig. 7. To verify the flow model, the simulated result of the spring-back angle was compared with the simulation and experimental values obtained from Lee's work [35], as shown in Fig. 8.

Fig. 7 shows that the largest value of effective strain for the material is 0.2835. The largest effective strain values for ferrite and martensite are 0.3677 and 0.0173,

respectively. Base on Eq. 1 and parameters in Table 1, if the effective strain value of the material is 0.2835, the corresponding effective strain values of ferrite and martensite are 0.3677 and 0.0173, respectively. This means that the simulation and calculation results are almost the same.

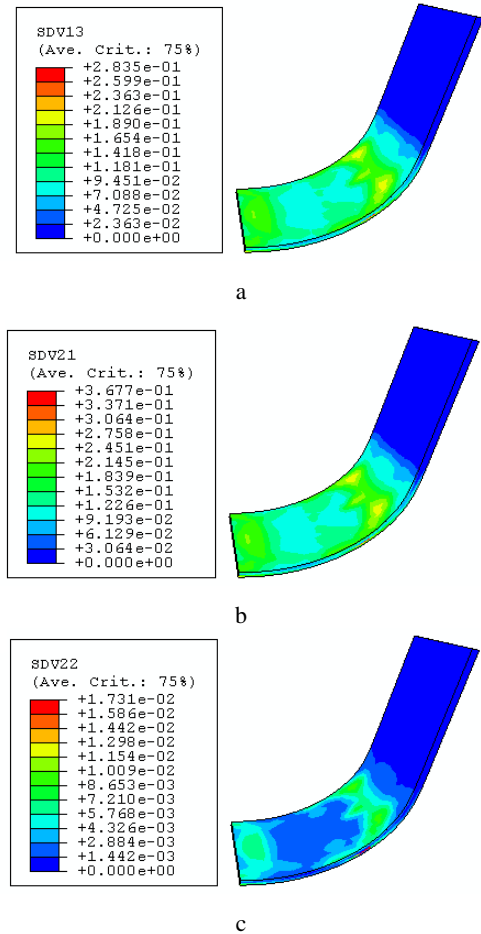


**Fig. 7.** Strain distribution of the material and individual phase after spring-back of the unconstrained cylindrical bending: a – material; b – ferrite; c – martensite

From Fig. 8, the spring-back angle of the unconstrained cylindrical bending in the experiment is 55.827 degree obtained from [35], while the angle calculated by the multi-phase constitutive model is 60.32 degree. The error between the simulated and calculated results is about 8% because of the Bauschinger effect was not considered during the process of the spring-back.

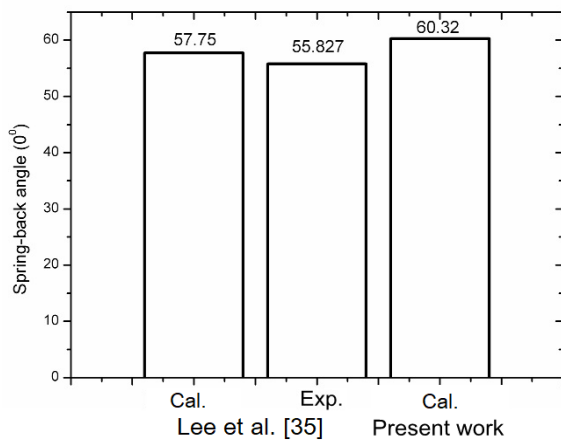


**Fig. 8.** Comparison of spring-back angles of the unconstrained cylindrical bending

#### 4.3. Verification of the flow model

The cup deep-drawing forming simulation shows that the steel strength is determined mainly by the hard martensite phase and the deformation of the material depends mostly on the soft ferrite phase. Moreover, it was found that high martensite content can improve the steel strength significantly but worsen the formability of the steel. The simulated results of the cup deep-drawing forming are consistent with the previous works of literature [36–41]. Meanwhile, the predicted spring-back angle of the flow model was in good agreement with the experimental and Lee's results under the unconstrained cylindrical bending forming. Thus, the flow model can predict the macro/micromechanical properties and the forming behavior of the investigated steel precisely.

#### 5. CONCLUSIONS

To describe the mechanical and forming behavior of ferrite-martensite DP steels precisely, an innovative flow model incorporating the mixture hardening law, anisotropic yield function, and incremental strain formulations was elaborated and applied to DP590 steel. The following conclusions can be drawn based on the results discussed in this work:

1. For the cup deep-drawing, both the effective stresses of the steel and martensite increase with increasing the martensite volume fraction, whereas the ferrite stress generally decreases. The effective strains of the material and two individual phases both at the bottom and punch round of the cup are positively related to the martensite volume fraction, while the strain is negatively related to the martensite volume fraction at the other parts of the cup. The results further prove that high martensite volume fraction would improve the material strength but deteriorate the formability of DP steels.
2. For the unconstrained cylindrical bending, the maximum simulated effective strains of the material and two individual phases are almost the same as the calculated results from Eq. 1. It was found that the spring-back angle error between the simulated and experimental results was about 7% because the Bauschinger effect in spring-back was not considered

in the incremental formulation for the ferrite-martensite DP steels.

3. The validity of the investigated model was verified by the stress/strain distribution in the cup deep-drawing and the spring-back angle in unconstrained cylindrical bending. The results reveal that the model is suitable to evaluate the mechanical behaviors of ferrite-martensite DP steels, e.g., the macro/micro effective stresses and strains, and the forming properties of DP steels both under the cup deep-drawing forming and unconstrained cylindrical bending.

#### Acknowledgments

This work was supported by the Anhui University Provincial Natural Science Research Project (KJ2018A0524), the Anhui University Provincial Outstanding Top-notch Talent Training Funded project (gxyq2018051) and the Key Discipline Team (AKZDXK2015C03).

#### REFERENCES

1. Hosseini-Toudeshky, H., Anbarlooie, B., Kadkhodapour, J. Micromechanics Stress-strain Behavior Prediction of Dual Phase Steel Considering Plasticity and Grain Boundaries Debonding *Materials & Design* 68 2015: pp. 167–176. <https://doi.org/10.1016/j.matdes.2014.12.013>
2. Ramazani, A., Mukherjee, K., Quade, H., Prah, U., Bleck, W. Correlation Between 2D and 3D Flow Curve Modelling of DP Steels Using a Microstructure-based RVE Approach *Materials Science and Engineering A-Structural Materials Properties Microstructure and Processing* 560 2013: pp. 129–139. <https://doi.org/10.1016/j.msea.2012.09.046>
3. Ramazani, A., Pinard, P.T., Richter, S., Schwedt, A., Prah, U. Characterisation of Microstructure and Modelling of Flow Behaviour of Bainite-aided Dual-phase Steel *Computational Materials Science* 80 2013: pp. 134–141. <https://doi.org/10.1016/j.commatsci.2013.05.017>
4. Choi, K.S., Liu, W.N., Sun, X., Khaleel, M.A., Ren, Y., Wang, Y.D. Advanced Micromechanical Model for Transformation-induced Plasticity Steels with Application of In-Situ High-Energy X-Ray Diffraction Method *Metallurgical and Materials Transactions A-Physical Metallurgy and Materials Science* 39 2008: pp. 3089–3096. <https://doi.org/10.1007/s11661-008-9649-4>
5. Choi, K.S., Liu, W.N., Sun, X., Khaleel, M.A. Micro structure-based Constitutive Modeling of TRIP Steel: Prediction of Ductility and Failure Modes under Different Loading Conditions *Acta Materialia* 57 2009: pp. 2592–2604. <https://doi.org/10.1016/j.actamat.2009.02.020>
6. Kim, J.H., Lee, M.G., Kim, D., Matlock, D.K., Wagoner, R.H. Hole-expansion Formability of Dual-phase Steels using Representative Volume Element Approach with Boundary-Smoothing Technique *Materials Science and Engineering A-Structural Materials Properties Microstructure and Processing* 527 2010: pp. 7353–7363. <https://doi.org/10.1016/j.msea.2010.07.099>
7. Uthaisangasuk, V., Muenstermann, S., Prah, U., Bleck, W., Schmitz, H.P., Pretorius, T. A study of

- Microcrack Formation in Multiphase Steel using Representative Volume Element and Damage Mechanics *Computational Materials Science* 50 2011: pp.1225–1232.  
<https://doi.org/10.1016/j.commatsci.2010.08.007>
8. **Uthaisangsuk, V., Prah, U., Bleck, W.** Characterisation of Formability Behaviour of Multiphase Steels by Micromechanical Modeling *International Journal of Fracture* 157 2009: pp. 55–69.  
<https://doi.org/10.1007/s10704-009-9329-4>
  9. **Eshelby, J.D.** The Determination of the Elastic Field of an Ellipsoidal Inclusion, and Related Problems *Proceedings of the Royal Society A* 241 (1226) 1957: pp. 376–396.  
<https://doi.org/10.1098/rspa.1957.0133>
  10. **Mori, T., Tanaka, K.** Average Stress in Matrix and Average Elastic Energy of Materials with Misfitting Inclusions *Acta Metallurgica* 21 1973: pp.571–574.  
[https://doi.org/10.1016/0001-6160\(73\)90064-3](https://doi.org/10.1016/0001-6160(73)90064-3)
  11. **Benveniste, Y.** A New Approach to the Application of Mori-Tanaka's Theory in Composite Materials *Mechanics of Materials* 6 1987: pp. 147–157.  
[https://doi.org/10.1016/0167-6636\(87\)90005-6](https://doi.org/10.1016/0167-6636(87)90005-6)
  12. **Hill, R.** A Self-consistent Mechanics of Composite Materials *Journal of the Mechanics and Physics of Solids* 13 1965: pp. 213–222.  
[https://doi.org/10.1016/0022-5096\(65\)90010-4](https://doi.org/10.1016/0022-5096(65)90010-4)
  13. **Lani, F., Furnémont, Q., Jacques, P.J., Delannay, F., Pardoën, T.** Micromechanical Modeling of Plastic Anisotropy and Strain Induced Phase Transformation in Dual-elastoplastic Phase Materials *Journal De Physique Iv* 105 2003: pp. 139–147.  
<https://doi.org/10.1051/jp4:20030181>
  14. **Lin, P.C., Lin, S.H., Pan, J.** Modeling of Failure Near Spot Welds in Lap-shear Specimens Based on a Plane Stress Rigid Inclusion Analysis *Engineering Fracture Mechanics* 73 2006: pp. 2229–2249.  
<https://doi.org/10.1016/j.engfracmech.2006.03.017>
  15. **Xu, F.Y., Bai, B.Z., Fang, H.S.** Influences of Volume Fraction, Shape and Strength of Martensite Islands on Mechanical Properties of Granular Structure Steels *Acta Metallurgica Sinica* 44 2008: pp. 1183–1187. (In Chinese)  
<https://doi.org/10.3321/j.issn:0412-1961.2008.10.007>
  16. **Tsuchida, N., Tomota, Y.** A Micromechanic Modeling for Transformation Induced Plasticity in Steels *Materials Science and Engineering A-Structural Materials Properties Microstructure and Processing* 285 2000: pp. 346–352.  
[https://doi.org/10.1016/S0921-5093\(00\)00688-2](https://doi.org/10.1016/S0921-5093(00)00688-2)
  17. **Garion, C., Skoczen, B., Sgobba, S.** Constitutive Modelling and Identification of Parameters of the Plastic Strain-induced Martensitic Transformation in 316L Stainless Steel at Cryogenic Temperatures *International Journal of Plasticity* 22 2006: pp. 1234–1264.  
<https://doi.org/10.1016/j.ijplas.2005.08.002>
  18. **Skoczen, B.** Functionally Graded Structural Members Obtained via the Low Temperature Strain Induced Phase Transformation *International Journal of Solids and Structures* 44 2007: pp. 5182–5207.  
<https://doi.org/10.1016/j.ijsolstr.2006.12.032>
  19. **Delannay, L., Jacques, P., Pardoën, T.** Modelling of the Plastic Flow of Trip-aided Multiphase Steel Based on an Incremental Mean-field Approach *International Journal of Solids and Structures* 45 2008: pp. 1825–1843.  
<https://doi.org/10.1016/j.ijsolstr.2007.10.026>
  20. **Sitko, M., Skoczen, B., Wróblewski, A.** FCC-BCC Phase Transformation in Rectangular Beams Subjected to Plastic Straining at Cryogenic Temperatures *International Journal of Mechanical Sciences* 52 2010: pp. 993–1007.  
<https://doi.org/10.1016/j.ijmecsci.2010.03.015>
  21. **Peng, X., Fan, J., Yang, Y.** A Micro Structure-based Description for Cyclic Plasticity of Pearlitic Steel with Experimental Verification *International Journal of Solids and Structures* 39 2002: pp. 419–434.  
[https://doi.org/10.1016/S0020-7683\(01\)00223-2](https://doi.org/10.1016/S0020-7683(01)00223-2)
  22. **Berbenni, S., Favier, V., Lemoine, X., Berveiller, M.** Micromechanical Modeling of the Elastic-viscoplastic Behavior of Polycrystalline Steels Having Different Microstructures *Materials Science and Engineering A-Structural Materials Properties Microstructure and Processing* 372 2004: pp. 128–136.  
<https://doi.org/10.1016/j.msea.2003.11.010>
  23. **Jia, N., Peng, R.L., Wang, Y.D., Chai, G.C., Johansson, S., Wang, G., Liaw, P.K.** Interactions between the Phase Stress and the Grain-orientation-dependent Stress in Duplex Stainless Steel during Deformation *Acta Materialia* 54 2006: pp. 3907–3916.  
<https://doi.org/10.1016/j.actamat.2006.04.019>
  24. **Franz, G., Abed-Meraim, F., Zineb, T.B., Lemoine, X., Berveiller, M.** Role of Intragranular Microstructure Development in the Macroscopic Behavior of Multiphase Steels in the Context of Changing Strain Paths *Materials Science and Engineering A-Structural Materials Properties Microstructure and Processing* 517 2009: pp. 300–311.  
<https://doi.org/10.1016/j.msea.2009.03.074>
  25. **Long, X.S., Peng, X.H., Pi, W.L.** A Microstructure-based Analysis of Cyclic Plasticity of Pearlitic Steels with Hill's Self-consistent Scheme Incorporating General Anisotropic Eshelby Tensor *Acta Mechanica Sinica* 24 2008: pp. 91–99.  
<https://doi.org/10.1007/s10409-007-0120-3>
  26. **Fan, J.** A Micro/macroscopic Analysis for Cyclic Plasticity of Dual-phase Materials *Journal of Applied Mechanics-Transactions of the ASME* 66 1999: pp. 124–136.  
<https://doi.org/10.1115/1.2789139>
  27. **Lee, M.G., Kim, D., Kim, C., Wenner, M.L., Wagoner, R.H., Chung, K.** Spring-back Evaluation of Automotive Sheets Based on Isotropic-kinematic Hardening Laws and Non-quadratic Anisotropic Yield Functions Part II: Characterization of Material Properties *International Journal of Plasticity* 21 2005: pp. 883–914.  
<https://doi.org/10.1016/j.ijplas.2004.05.015>
  28. **Huh, H., Kim, S.B., Song, J.H., Lim, J.H.** Dynamic Tensile Characteristics of TRIP-type and DP-type Steel Sheets for an Auto-body *International Journal of Mechanical Sciences* 50 (5) 2008: pp. 918–931.  
<https://doi.org/10.1016/j.ijmecsci.2007.09.004>
  29. **Kang, J., Ososkov, Y., Embury, J.** Digital Image Correlation Studies for Microscopic Strain Distribution and Damage in Dual Phase Steels *Scripta Materialia* 56 2007: pp. 999–1002.  
<https://doi.org/10.1016/j.scriptamat.2007.01.031>
  30. **Tasan, C.C., Hoefnagels, J.P.M., Geers, M.G.D.** Microstructural Banding Effects Clarified Through Micrographic Digital Image Correlation *Scripta Materialia* 62 2010: pp. 835–838.  
<https://doi.org/10.1016/j.scriptamat.2010.02.014>
  31. **Ghadbeigi, H., Pinna, C., Celotto, S.** Local Plastic Strain Evolution in a High Strength Dual-phase Steel *Materials*

- Science and Engineering A-Structural Materials Properties Microstructure and Processing* 527 2010: pp. 5026–5032. <https://doi.org/10.1016/j.msea.2010.04.052>
32. **Dan, W.J., Lin, Z.Q., Li, S.H., Zhang, W.G.** Study on the Mixture Strain Hardening of Multi-phase Steels *Materials Science and Engineering A-Structural Materials Properties Microstructure and Processing* 552 2012: pp. 1–8. <https://doi.org/10.1016/j.msea.2012.04.028>
  33. **Dan, W.J., Zhang, W.G., Li, S.H., Lin, Z.Q.** A Model for Strain Induced Martensitic Transformation of TRIP Steel with Strain Rate *Computational Materials Science* 40 2007: pp. 101–107. <https://doi.org/10.1016/j.commatsci.2006.11.006>
  34. **Dan, W.J., Zhang, W.G., Liu, F.** Constitutive Model for Multi-phase High Strength Steels *Procedia Engineering* 81 2014: pp. 1204–1209. <https://doi.org/10.1016/j.proeng.2014.10.098>
  35. **Lee, M.G., Kim, D., Kim, C., Wenner, M.L., Chung, K.** Spring-back Evaluation of Automotive Sheets Based on Isotropic-kinematic Hardening Laws and Non-quadratic Anisotropic Yield Functions Part III: Application *International Journal of Plasticity* 21 2005: pp. 915–953. <https://doi.org/10.1016/j.ijplas.2004.05.014>
  36. **Zhou, L.Y., Jiang, B., Cui, T.H., Zhang, D., He, J.Z., Liu, Y.Z.** Effect of Strengthening Phase on Deformation Behaviour during Uniaxial Tension of Hot-rolled Dual Phase Steel *Journal of Iron and Steel Research, International* 21 (12) 2014: pp. 1111–1115. [https://doi.org/10.1016/S1006-706X\(14\)60191-6](https://doi.org/10.1016/S1006-706X(14)60191-6)
  37. **Byun, T.S., Kim, I.S.** Tensile Properties and Inhomogeneous Deformation of Ferrite-Martensite Dual-Phase Steels *Journal of Materials Science* 28 1993: pp. 2923–2932. <https://doi.org/10.1007/BF00354695>
  38. **Davies, R.G.** Influence of Martensite Composition and Content on the Properties of Dual Phase Steels *Metallurgical Transactions A* 9 1978: pp. 671–679. <https://doi.org/10.1007/BF02659924>
  39. **Asadi, M., De Cooman, B.C., Palkowsk, H.** Influence of Martensite Volume Fraction and Cooling Rate on the Properties of Thermomechanically Processed Dual Phase Steel *Materials Science and Engineering A-Structural Materials Properties Microstructure and Processing* 538 2012: pp. 42–52. <https://doi.org/10.1016/j.msea.2012.01.010>
  40. **Mazinani, M., Poole, W.J.** Effect of Martensite Plasticity on the Deformation Behavior of a Low-Carbon Dual-Phase Steel *Metallurgical and Materials Transactions A* 38 2007: pp. 328–339. <https://doi.org/10.1007/s11661-006-9023-3>
  41. **Lai, Q., Brassart, L., Bouaziz, O., Gouné, M., Verdier, M., Parry, G., Perlade, A., Bréchet, Y., Pardoën, T.** Influence of Martensite Volume Fraction and Hardness on the Plastic Behavior of Dual-phase Steels: Experiments and Micromechanical Modeling *International Journal of Plasticity* 80 2016: pp.187–203. <https://doi.org/10.1016/j.ijplas.2015.09.006>



© Gou et al. 2020 Open Access This article is distributed under the terms of the Creative Commons Attribution 4.0 International License (<http://creativecommons.org/licenses/by/4.0/>), which permits unrestricted use, distribution, and reproduction in any medium, provided you give appropriate credit to the original author(s) and the source, provide a link to the Creative Commons license, and indicate if changes were made.